International Journal of Engineering and Advanced Technology (IJEAT)
ISSN: 2249-8958 (Online), Volume-2 Issue-4, April 2013

Assessment of the Tensile Elongation (E %) And Hardening Capacity (Hc) Of Joints Produced In Friction Stir Welded 2017 Aa (Enaw-Alcu 4mgsi) Plates

Ali Trabelsi, Mohamed-Ali Rezgui And Smain Bezzina

Abstract*— The study has aimed at investigating the leverage of three Friction Steer Welding (FSW) factors, namely, the tool rotation speed N(rpm), the tool traverse rate F(mm.mn^{-1}) and the tool pin/shoulder diameters ratio r (%) on two FSW process responses: the joint tensile elongation (E%) and hardening capacity (Hc). For the experiment appraisal, 18 tested coupons have been cut in 6mm thick rolled plates of 2017 A alloys. Variation in the responses estimates has been assessed by conducting a Face-Centered Central Composite Design (FCCD) strategy and Anova Technique. Then, a second-order RSM model has been considered to describe the predictive formulation of the responses (E%) and (Hc), appropriately. Thereby, the multi-regression models pertaining to (E%) and (Hc) were built and analyzed for factors leverage and sensitivity. Lastly, a simultaneous optimization procedure based on the desirability function was employed to find out the levels setting of factors N, F and r% which guarantees maximum (E%) and (Hc), concurrently.

At 95% of C.I., the research findings have pointed out the leverage of the tool geometry factor (r %) as well as the rotation speed (N) on the FSW process responses (E%) and (Hc). However, the process was found robust with respect to the tool traverse rate parameter (F).

Keywords- F.S.W., R.S.M., Taguchi, ANN, Genetic Algorithms, Ductility, Tensile elongation, Hardening capacity, 2017 AA.

I. INTRODUCTION

As it is known today, the Friction Stir Welding (FSW) technique emerged in the 90's and has been patented by the TWI [1]. The process has found broad use in numerous industrial fields (e.g., automotive, aerospace, military, petro-chemical, etc.). When compared with conventional fusion welding, the FSW has the ability to produce joints which experience higher strength and formability [2,3]. Mainly, this is because of the low welding temperature supply brought to the weld nugget (WN), the thermo-mechanically affected zone (TMAZ) and the heat affected zone (HAZ). The FSW has also proven superior to produce crack and porosity free joints and better deals with materials which possess poor fusion weld ability [4,5] (e.g., the 2xxx and 7xxx series of the heat treatable aluminum). In Nadan et al [6], a thorough review of the basic design and microstructure characteristics which are relevant to the plastic deformation, frictional heat, tool design as well as the perception weld zones has been discussed.

Basically, the FSW process employs a tool pin/probe which plunges into the interface of a set of sheets/plates to be welded. After that, the tool tracks the joint direction to execute the weld. Mechanically, the interface region metal is heated and stirred, mainly, by: i) undergoing the weld joint zones a friction energy under the shoulder loading, ii) and, malaxation of the softened material using the pin movement. FSW has concerned similar, dissimilar [7] as well as metal matrix composites [8]. Though, because of the frictional and stirring effect of the tool pin, softening of some welded materials may occur, hence, giving rise to a manifest change of the mechanical properties of joints. Recently, a non-rotational shoulder assisted FSW technique [9] has been put in practice wherein the micro-structural deformation and the weld formation were dominated by the rotating tool pin, solely.

Much research has addressed the microstructure and estimate of the mechanical properties of FSWed joints. Purposely, some studies have tackled the influence of the tool rotation rate and/or the welding speed [10, 11]. Others have considered the tool geometry [12, 13]. Major findings have pointed out the leverage of the materials, experimental equipment and the designs of the stirring tools on the mechanical properties of the produced joints [14]. One challenge, however, is how FSW parameters could be fixed so that high quality joints are produced cost-effectively. Statistical techniques, among other solutions, have brought substantial contribution in this regard. These are organized into four classes, i) factorial design and Anova [15, 16], ii) RSM [17, 18, 19], iii) Taguchi method [20, 21], iv) and, ANN & Genetic method [22, 23].

For the Aluminum alloys, even though, much literature has coped with the microstructure analysis and the estimate of the mechanical properties of FSWed joints, only, a little has concerned the 2017 AA [24, 25]. This is despite of its good machinability and formability. Table 1 enlists the 2017 AA B.M. nominal mechanical characteristics which have been considered in this study.

Table 1. Mechanical properties of the 2017 AA (B.M)

Base Metal (BM) 2017A (ENAW-AlCu4MgSi)	UTS (MPa)	YS (MPa)	E (%)

Manuscript published on 30 April 2013.
***** Correspondence Author (s)
Ali TRABELSI, Dept. of Mechanical Engineering, High National School of Engineering of Tunis, Tunisia.
Mohamed-Ali REZGUI, College of Engineering, Taibah University, Yanbu-Branch, Saudi Arabia.
Smain BEZZINA, University of Khemis Miliana, Algeria.

Mechanical properties	427	276	22
Chemical Composition (%)	Fe<0.7427	Si. 0.2-0.8	Mn. 0.4-1.0
	Cr<0.1	Cu. 3.5-5.5	Mg. 0.4-1.0
	Zn<0.25	(Zr+Ti)<0.25	Al. remainder

The study purposes to build up predictive models of the FSW responses (E%) and (Hc) in N, F and r%. The experiment has been conducted in a sequential strategy. First, a 2^3 full factorial plan has been run to fit linear regression models. Then, owing to lack of fit, the design has been augmented by six axial and four center point runs (FCCD) to fit second order RSM models. These have proven fitting as it will be explained further. The Anova and the partial derivative techniques were employed to test out, i) factors which have significant influence on the process variability within their exploration spaces, ii) and, the sensitivity of factors N, F and r% on the FSW responses (E%) and (Hc), that is, the magnitude and direction of changes in the process outputs whenever an *infinitesimal* variation in the input(s) occurred. Finally, the study has addressed the simultaneous optimization of the process responses, E% and Hc, such that factors setting would yield maximum estimates of (E%) and (Hc), simultaneously.

The remaining text is structured as it follows. Section II presents the study experimental framework and lies out findings pertaining to the true stress-strain curves of the tested specimens. The base metal (BM) mechanical characteristics were used for comparison. Section III experiences the empirical models pertaining to the FSW responses (E%) and (Hc). Finally, section IV discusses findings regarding the optimization procedure.

II. EXPERIMENTAL FRAMEWORK

A. Set up and true stress-strain curves of specimens

The FSW experiment has employed a 7.5 kw powered universal mill (Momac model), rating up to 1700 rpm of rotation speed and 1080 $mm.mn^{-1}$ of feed rate. A series of 6 mm thick rolled plates of 2017 AA were cut into 250x90 mm rectangular dimensions and disposed in butt configuration for FSW. The plates are held using a metal frame which is in turn clamped on the mill table as it is visualized in Fig. 1. The welding tools were manufactured in a high steel alloy (35 HR C). Fig. 2 shows the tools used in this experiment as well as the shoulder/pin geometry.

Fig.1. Photography of the FSW setting frame.

Lastly, the FSW plates were cross-sectioned and the specimens were prepared for the tensile test. Insofar, the factorial runs are deemed $F_{i=1,8}$, the center point runs, $C_{i=1,4}$ and the axial runs, $A_{i=1,6}$ as shown in Fig 3.

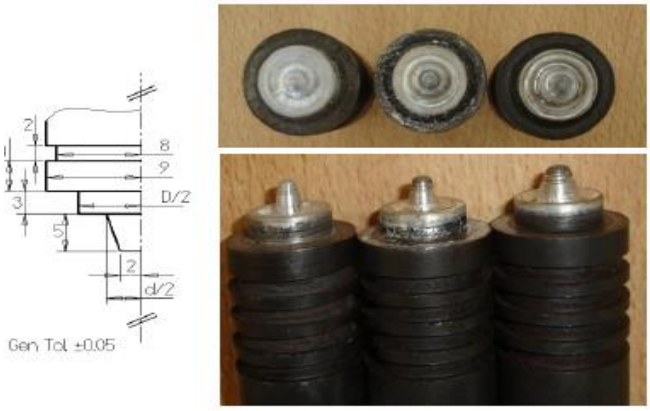

Fig. 2. Experiment tools and shoulder/pin geometry.

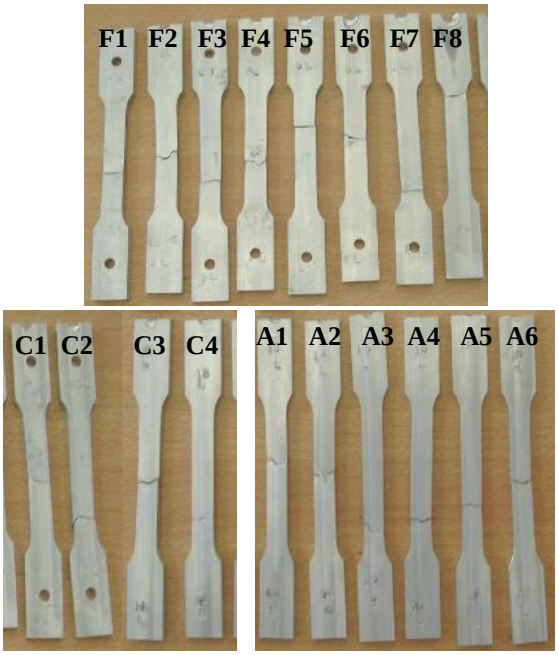

Fig. 3. Specimens and zones of fracture after tensile tests. $F_{i=1,8}$ factorial runs, $C_{i=1,4}$ center point runs, and $A_{i=1,8}$ star point runs

Each specimen has been prepared according to the ASME E8M-04 standard and, have been undergone a tensile test at room temperature and at a crosshead speed of $0.1mm.mn^{-1}$. Among the 18 tested samples, nine have failed midway the gauge length and six broken in the vicinity of the grip region. In Fig. 4a, 4b and 4c, the true stress-strain curves of the specimens put side by side the base metal (BM) plot are given. Manifestly, all specimens have similar true tress-train plots with (σ_{UTS}) and (σ_{YS}) lesser than what it has been found for the BM. In average, a decrease of 39% in the (σ_{UTS}) and 17% in (σ_{YS}) was observed given the BM characteristics. And, maximum (σ_{UTS}) and (σ_{YS}) were achieved at about 59% and 24% of the BM performances [26].

Published By:
Blue Eyes Intelligence Engineering
and Sciences Publication (BEIESP)

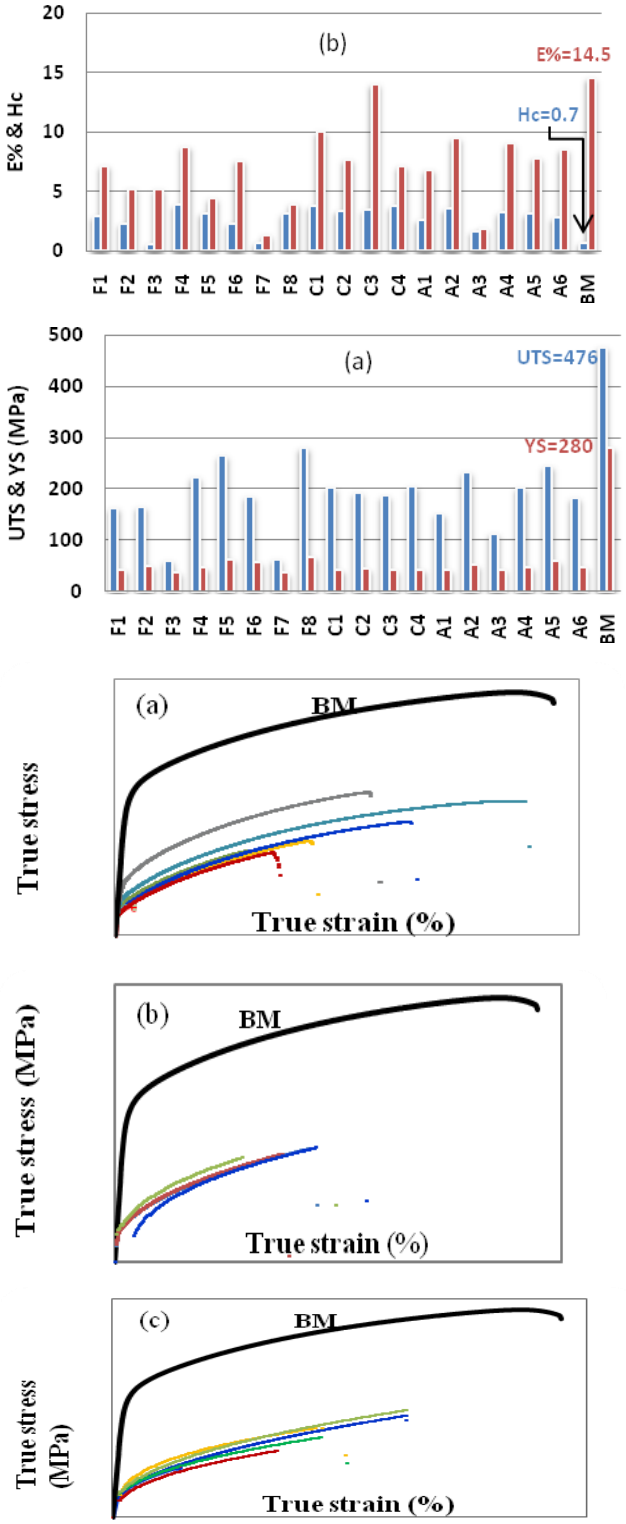

Fig. 4. True stress-strain plots of the specimens *versus* the B.M. (a) Factorial, (b) Center, (c) Star runs.

The plots in Fig. 5a and 5b show the (σ_{UTS}), (σ_{YS}), (Hc) and (E%) which have been measured in the specimens and compared with the BM. The C3 run in Fig.5.b holds rather a suspicious tensile elongation in comparison with the BM. This could stand for an outlier point which when looking into did not question the experiment data integrity.

A. *Experiment strategy*

Response surface methodology (RSM) has been broadly implemented to formulate functional relationship (*a priori* unknown) between dependent process responses and the independent process parameters variables [27]. Because we suspected curvature in the functional relationship, we decided on fitting second order models. Accordingly, the experiment has been conducted in 18 CCD ($\alpha=\pm1$) runs. For the DoE coding, the actual units of the –1 and +1 levels are set at 653 r.p.m and 1280 r.p.m for the rotation speed (N), 67 mm.mn^{-1} and 109 mm.mn^{-1} for the tool traverse rate and, 33% and 44% for the tool diameters ratio (r%). The intermediate setting of N, F and r% has been maintained at 910 r.p.m, 86 mm.mn^{-1} and 39%, respectively. Table 2 enlists the process parameters as well as the setting levels recipe.

Fig. 5.Mechanical properties of the tested specimens and the B.M. a) (σ_{UTS}) and (σ_{YS}), b) (Hc) and (E%).

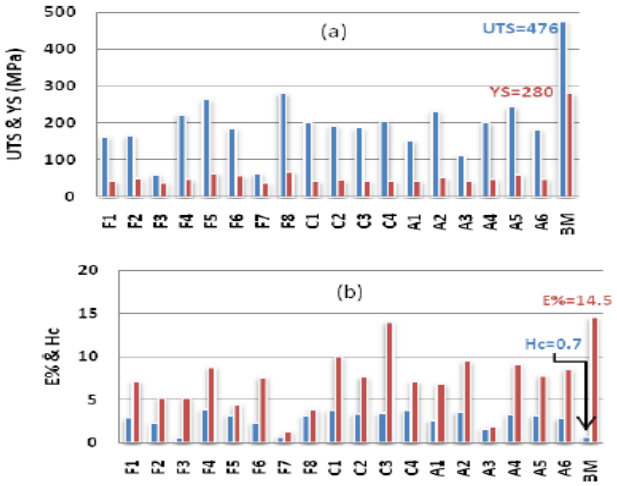

Because nuisance factors are present and must be accounted for, five controllable factors have been chosen and held constant all through the experiment time. Table 3 enlists the nuisance factors hold for the experiment.

The design encoding, Anova tables as well as the sensitivity/optimization analysis will be assisted using Minitab® software. Table 4 shows the study DoE layout as expressed in natural coding units.

Table 3. FSW process parameters maintained constant

Parameters	Value
Pin height (mm)	5.3
Shoulder diameter (mm)	18
Pin small cone diameter(mm)	4
Tool inclination (°)	3
Infeed (mm)	0.94

Table 4. CCD layout for the FSW process experiment

Factors Setting FCCD (8 factorial + 4 Center + 6 Axial runs)						Process Responses			
Std. Ord.	Run Ord.	Pts. Types	N rpm	F mm.mn^{-1}	r (%)	E%	[26] σ_{UTS}	[26] σ_{ys}	Hc = $\frac{\sigma_{UTS}}{\sigma_{YS}}$-1
17	1	0	910	86	39	7.150	202.5	42.5	3.765
7	2	1	653	109	44	5.200	163.0	42.0	2.881
14	3	-1	910	86	44	5.140	151.0	42.0	2.595
9	4	-1	653	86	39	8.760	232.0	51.0	3.549
2	5	1	1280	67	33	4.400	165.0	50.0	2.300
16	6	0	910	86	39	7.600	192.0	44.0	3.364
6	7	1	1280	67	44	1.300	60.0	38.0	0.579
10	8	1	1280	86	39	3.930	113.0	43.0	1.628
5	9	-1	653	67	44	10.000	223.0	46.0	3.848
11	10	1	910	67	39	7.660	202.0	48.0	3.208
3	11	-1	653	109	33	14.000	264.0	63.0	3.190
15	12	1	910	86	39	7.100	186.0	42.0	3.429
4	13	0	1280	109	33	6.800	185.0	56.0	2.304
13	14	-1	910	86	33	9.460	244.0	59.0	3.136
8	15	1	1280	109	44	1.900	62.0	36.0	0.722
1	16	1	653	67	33	9.000	280.0	68.0	3.118
12	17	-1	910	109	39	7.810	182.0	48.0	2.792
18	18	0	910	86	39	8.500	204.0	43.0	3.744

Published By:
Blue Eyes Intelligence Engineering
and Sciences Publication (BEIESP)

EXPERIMPIRICAL PREDICTIVE MODELS

A. The predictive model for the tensile elongation (E%)

Beforehand, we emphasized a quadratic RSM model which is able to describe variation in the tensile elongation response (E%), reliably, will be experienced. Allowing for a threshold of 95% C.I., the candidate regression model(s) should satisfy the best trade-off among the model statistics, that is, the LoF, R^2, R^2-pred, R^2-adj and S.

Table 5. Regression models of (E%) and (Hc) in N, F and r% (candidate sub-sets are highlighted in bolt).

	Model Terms	Model Statistics				
		S	R^2	R^2 (pred)	R^2 (adj)	LoF
(E%) model	N, F, r%	1.46	80.86	58.45	76.76	0.080
	N, r%	1.44	80.19	66.53	77.55	0.990
	N, F, r%, NxF, Fxr%, Nxr%	1.05	92.25	17.06	88.02	0.180
	N, F, r%, Fxr%	**1.00**	**91.63**	**75.11**	**89.06**	**0.210**
	Full quadratic	1.12	93.56	0.00	86.31	0.134
(Hc) model	N, F, r%	0.62	66.24	36.81	59.01	0.040
	N	0.64	58.70	45.56	56.12	0.020
	N, F, r%, NxF, Fxr%, Nxr%	0.55	79.08	0.00	67.67	0.050
	N, r%, Nxr%	0.52	76.21	60.56	71.11	0.030
	Full quadratic	0.30	95.35	61.06	90.13	0.214
	N, r%, Nxr%, N^2	**0.36**	**89.40**	**80.36**	**86.14**	**0.420**

Accordingly, the (N, F, r%, NxF, Fxr%, Nxr%) model represents a potential candidate as it is indicated in Table 5 elucidates. Also, the four-plot shown in Fig. 6 charts the model residuals behavior and does not question the model adequacy, correspondingly. Yet, the residuals normality and the independence conjectures were found ostensibly violated (i.e., normality p-value 0.035<5% and the residual scattering is enlarged when factors F, N and r% are set middle). When referring to Table 5, the factors N, F and r% explain 80.19% to 93.56% of the variability in E%. And, the LoF of all inspected models advise insignificance at 5% level. Hence, suggesting that first order models are considered fit. The pure error standard deviation of the experiment ranges 1.003 to 1.46 and the lowest value (Std=1.003) was met for the (N, F, r%, Fxr%) model.

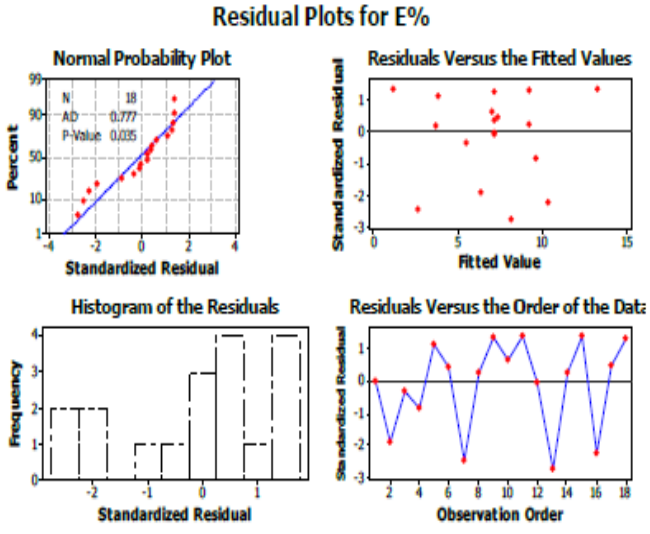

Fig. 6. Four-plots chart of the full model (main+ interaction effects).

The analysis of the (N, F, r%, NxF, Fxr%, Nxr%) model summary of fit is given in Appendix A. It uncovers a poor performance *vis-à-vis* the model capability to predict new data (R^2-(pred) 17.06%). Also, the Anova Table (Appendix A) indicates that at 95% of C.I., only the main effect of factors N and r% (p-value 0.000) and the interaction Fxr% (p-value 0.002) are statistically significant. Therefore, the reduced model (N, F, r% and Fxr%) was retained to describe variation in (E%). The model accounts for a LoF=0.214, R^2=91.63%, S=1.003 and R^2-(pred)=75.11%.

Given the exploration spaces pertaining to factors N, F and r%, the tensile elongation (E%) model can be expressed as it follows.

Coding units (1):

$$\hat{E}\% = 6.843 - 2.912(N) + 0.351(F) - 2.019(r\%) - 1.448(Fxr\%)$$

Natural units (2):

$$\hat{E}\% = -13.986 - 0.009(N) + 0.499(F) + 0.736(r\%) - 0.012(Fxr\%)$$

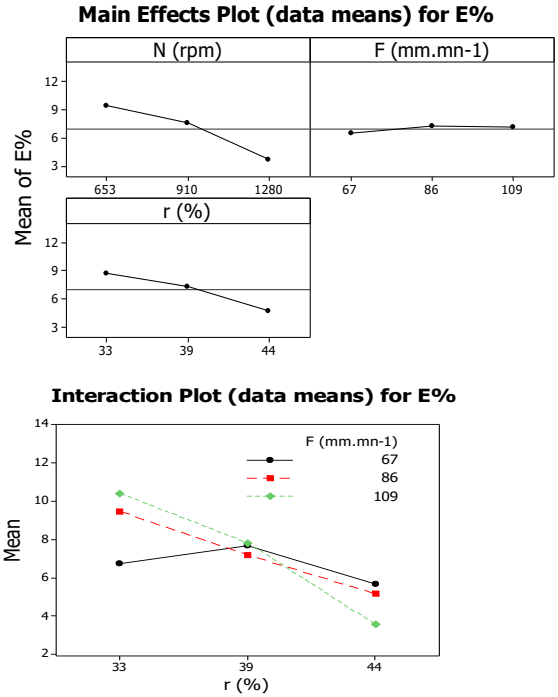

Fig. 7. Main and interaction plots for response(E%).

The interaction Fxr% is better manifested in Fig. 7 which represents the effect of the r% factor on the mean response (E%) for different setting of the tool traverse rate (F). The effect was small when (F) is set low and large when it is set middle or high, agreed r% ϵ [33%, 39%], with the best setting at F high and low r%. Interestingly, changing the r% setting from low to intermediate would result in almost the same mean response (E%) (about 7.49%) regardless of the traverse rate setting. From intermediate to high setting of r%, the mean response (E%) attains its maximum when F is set low. Furthermore, at 5% of type I error, the rotation speed (N) has a statistically significant effect on the response (E%) and it does not take part in any significant interaction.

Published By:
Blue Eyes Intelligence Engineering
and Sciences Publication (BEIESP)

Therefore, it is advisable to set N low as Fig. 7 suggests.

Presently, if we refer to the surface contour plot which is shown in Fig. 8, it is indicated the maximum mean elongation ($E\%_{max}$) was met for N, F and r% being set low (653 rpm), high (109 $mm.mn^{-1}$) and low (33%), respectively.

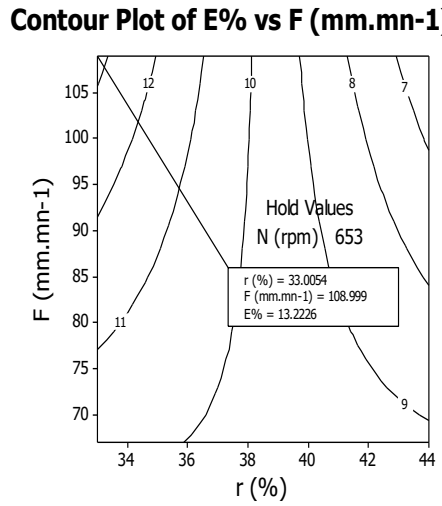

Fig. 8. Response surface contour plot of response (E%)

In Fig. 8, the surface contour plot for F high is shown and it is indicated the maximum elongation ($E\%_{max}$) is graphically achieved at about 13.223%.

So far, we determined the main and interaction effects of the N, F and r% process parameters on the response (E%). The reliability of the fitted model as expressed in equations (1) and (2) is further argued by getting insight into the most sensitive factors.

The calculation of the partial derivatives (direct method) of the regression model with respect to N, F, and r% is performed to determine the sensitivity coeficients $\phi_{i=N,F,r\%}$ of the independent variables N, F and r% on E%.

$$\phi_N = \frac{\partial \hat{E}\%}{\partial N}\frac{N}{\hat{E}\%} \quad (3)$$

$$\phi_F = \frac{\partial \hat{E}\%}{\partial F}\frac{F}{\hat{E}\%} \quad (4)$$

$$\phi_{r\%} = \frac{\partial \hat{E}\%}{\partial r\%}\frac{r\%}{\hat{E}\%} \quad (5)$$

The quotients $\frac{N}{\hat{E}\%}$, $\frac{F}{\hat{E}\%}$ and $\frac{r\%}{\hat{E}\%}$ are introduced to normalize the coefficients by removing the effects of units. The partial derivatives of (E%) with respect to N, F, and r% in active coding are given below:

$$10^2 \frac{\partial \hat{E}\%}{\partial N} = -9.290 \quad (6)$$

$$10^2 \frac{\partial \hat{E}\%}{\partial F} = 499.355 - 12.536(r\%) \quad (7)$$

$$10^2 \frac{\partial \hat{E}\%}{\partial r\%} = 735.957 - 12.536(F) \quad (8)$$

The partial derivatives of E% in respect of F and r% are linear in r% and F, respectively, and both have the same negative slop (-12.536). However, the partial derivative of E% in respect of N was found irrelevant to the factors N, F and r%, indistinctly.

For the sensitivity analysis (Fig. 9), the sensitivity coefficients

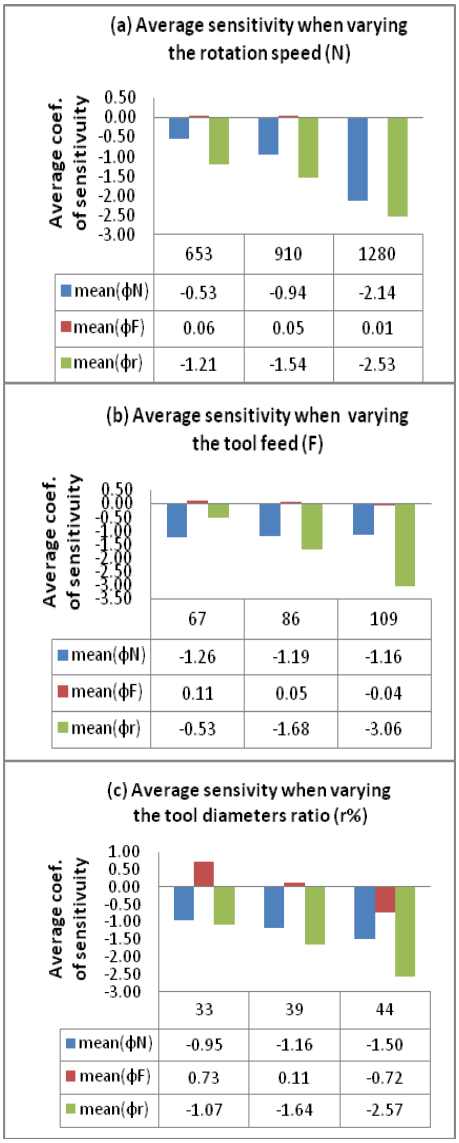

Fig.9. Sensitivity analysis for the process response (E%). a) when varying the tool rotation speed (N), b) when varying the traverse rate (F), c) and, when varying the tool diameters ratio (r%).

were calculated by averaging them over different factors setting. The histograms displayed in Fig. 9 suggest the following findings:

- In average, the tool traverse rate factor (F) is insensitive to the process response (E%) despite of the N, F and r% setting levels.
- Allowing for factors N and r%, the histograms in Fig. 9a, 9b and 9c, indicate that, in average, the tool diameters ratio (r%) is the major sensitive factor on (E%). The maximum sensitivity of r% is met when (F) is set high ($\phi_{r\%}$=-3.06). The sensitivity of N on (E%) is rather irrelevant to the traverse rate (F) and at a lesser degree to the r% setting level as it is shown in Fig. 9b and 9c. The histogram of Fig. 9a shows that the maximum sensitivity of N on (E%) occurs at the vicinity of N high (ϕ_N=-2.14).

Published By:
Blue Eyes Intelligence Engineering
and Sciences Publication (BEIESP)

- Local maximum sensitivity of N (ϕ_N=-3.2), F (ϕ_F=-1.53) and r% ($\phi_{r\%}$=-7.47) on (E%) were observed when N, F and r% are set high, altogether (see Appendix C).

Appendix C summarizes the calculation of the local sensitivity coefficients, $\phi_{N,\,Fr\%}$ for all combination of factors setting.

B. The predictive model for the hardening capacity (Hc)

The calculation of the hardening capacity response (Hc) has been initiated from the experimental data of (σ_{UTS}) and (σ_{YS}) [26] (see Table 4). The normalized form of the hardening capacity (Hc) [27] is given below.

$$H_C = \frac{\sigma_{UTS}}{\sigma_{YS}} - 1 \qquad (9)$$

Likewise the foregoing, we purpose to fit a quadratic RSM model which is able to assess variation in the (Hc) process response, reliably. The analysis of the first order and second order (main + interaction terms) regression models revealed inappropriate owing to LoF as it has been reported in Table 5 (i.e., all p-values are lesser than 5%). A full quadratic model is therefore thought of. The visual checking of the scattering plot of residuals of such a model is shown in Fig. 10 and does not suggest any abnormal patterns, yet, the residuals normality assumption (p-value<5%) is manifestly violated. The normality assumption is satisfied (p-value 0.417) when considering the reduced model (N, r%, Nxr%, N^2) as it will be explained further. The Appendix B gives a summary of the statistics for both the full and reduced quadratic models. The statistics sustain the full quadratic model ability to fit variation in (Hc), that is, LoF=0.214, R^2=95.35%, S=0.304 and R^2 (pred)=61.06%). However, the Anova Table highlights the leverage of the terms N (p-value 0.000), r% (p-value 0.006), N^2 (p-value 0.056) and the interaction Nxr (p-value 0.002) at 95% of C.I. Also, the regression p-values of the interactions (p=0.011) and the squared terms (p=0.005) are found statistically significant, suggesting presence of curvature in the response surface.

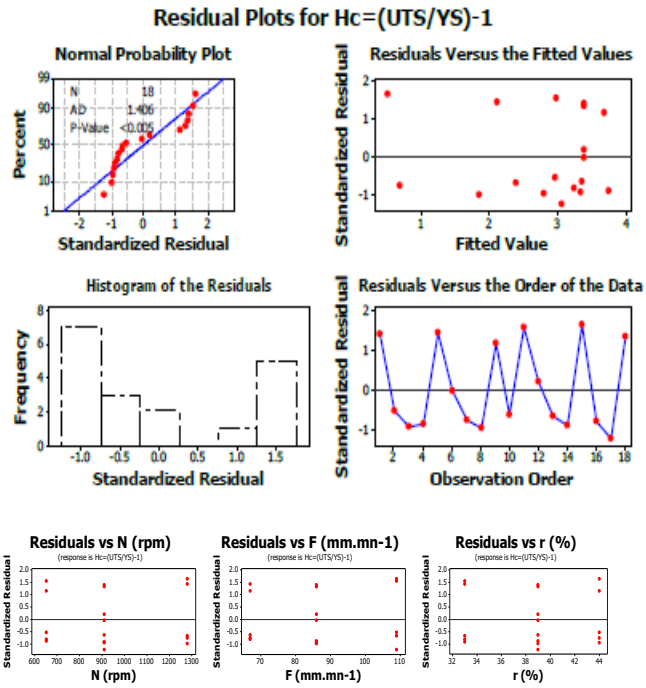

Fig. 10. Four-plots chart for the model adequacy of response (Hc)

Once we get rid of insignificant main and interactions terms, we obtained the reduced candidate model (N, r%, N^2 and Nxr%) which demonstrates better performances. From Table 5, we read a LoF=0.423, R^2=89.40%, S=0.360 and R^2 (pred)=80.36%. Notice the obvious increase in R^2-(pred) in comparison with that found for the full quadratic model.

Considering the exploration spaces of factors N, F and r%, the empirical model for the hardening capacity (Hc) can be formulated as it follows.

Coding units(10):

$$\hat{H}_C = 3.134 - 0.897(N) - 0.348(r\%) - 0.467(Nxr\%) - 0.715(N^2)$$

Natural units(equation 11):

$$\hat{H}_C = -8.548 + 0.022(N) + 0.199(r\%) - 2.710.10^{-4}(Nxr\%) - 7.279.10^{-6}(N^2)$$

The interaction plot shown in Fig. 11 displays the effect of r% on the mean response (Hc) which is found small when the rotation speed (N) is set high and large when the rotation speed is low, with the best setting at N low and r% middle. The Anova (see Appendix B) indicates the traverse rate (F) was irrelevant (p-value 0.288 at 5% of type I error) to the variation in (Hc), that is, the FSW process is robust to the traverse rate variation. From the main effect plot (see Fig. 11), it turns out that maintaining F at middle level (F=86 mm.mn^{-1}) would result in the highest average for (Hc). Hence, the best mean hardening capacity (Hc) is achieved at N, F and r% low (653 rpm), middle (86 mm.mn^{-1}) and middle (39%), respectively. Changing the r% setting level from low to intermediate brings about a small increase in the mean hardening capacity (Hc) for N low or middle and a rapid decrease in (Hc) for N high. And, changing r% from intermediate to high entails a drop in the mean hardening capacity (Hc) despite of the N setting level. Therefore, the maximum of the hardening capacity do occur when the rotation speed is set low. The contour plot displayed in Fig. 12 (traverse rate being maintained low) indicates that the maximum hardening capacity is attained at about Hc_{max}=3.822.

The Appendix B has given the statistical significant factors which impact the response (Hc), namely, the linear effect in N and r%, the interaction effect Nxr% and a quadratic effect in N^2. The reliability of the RSM model is further corroborated by getting insight the sensitive factors on the process response (Hc). Likewise before, we proceed by the calculation of the partial derivatives of (Hc) with respect to N, F, and r%.

The sensitivity coeficients for the independent variable N, F and r% are given below.

$$\phi_N = \frac{\partial \hat{H}_C}{\partial N}\frac{N}{\hat{H}_C} \qquad (12)$$

$$\phi_F = \frac{\partial \hat{H}_C}{\partial F}\frac{F}{\hat{H}_C} \qquad (13)$$

Published By:
Blue Eyes Intelligence Engineering
and Sciences Publication (BEIESP)

$$\phi_{r\%} = \frac{\partial \hat{H}_C}{\partial r\%} \frac{r\%}{\hat{H}_C} \qquad (14)$$

$\frac{N}{\hat{H}_c}$, $\frac{F}{\hat{H}_c}$ and $\frac{r\%}{\hat{H}_c}$ are introduced for normalization.

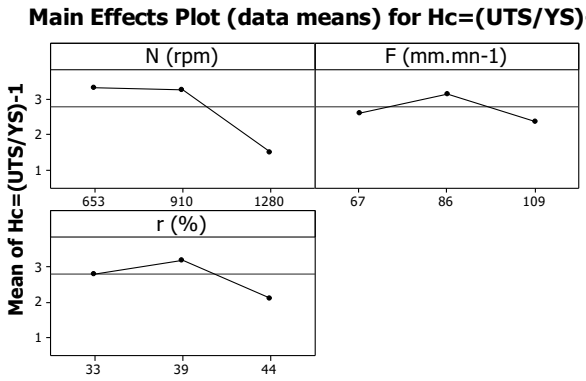

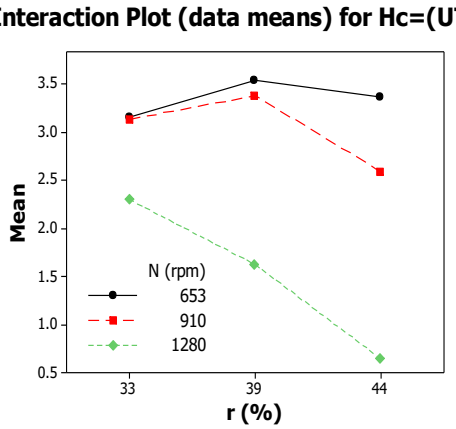

Fig. 11. Main and interaction plots of the FSW process response (Hc).

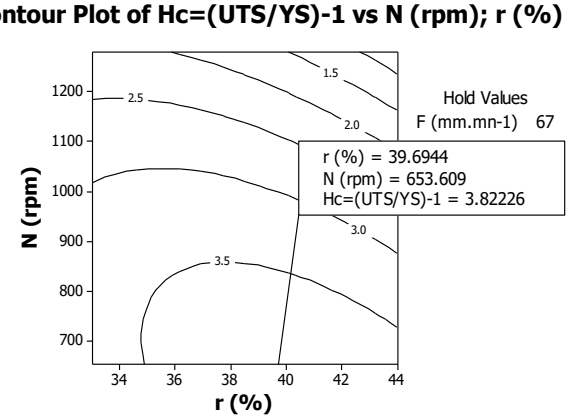

Fig. 12. Response surface and contour plot of (Hc).

The partial derivatives of (Hc) in respect of N, F and r% as expressed in active units are:

$$10^4 \frac{\partial \hat{H}_C}{\partial N} = 216.425 - 0.146(N) \qquad (15)$$

$$\frac{\partial \hat{H}_C}{\partial F} = 0 \qquad (16)$$

$$10^4 \frac{\partial \hat{H}_C}{\partial r\%} = 1986.340 - 2.710(N) \qquad (17)$$

Notice, the partial derivative in respect of F equals zero which means the FSW process is robust to the factor F when considering the hardening capacity. The Appendix C reports on the sensitivity coefficients of N, F, and r% on the process response (Hc) for all combination of factors setting.

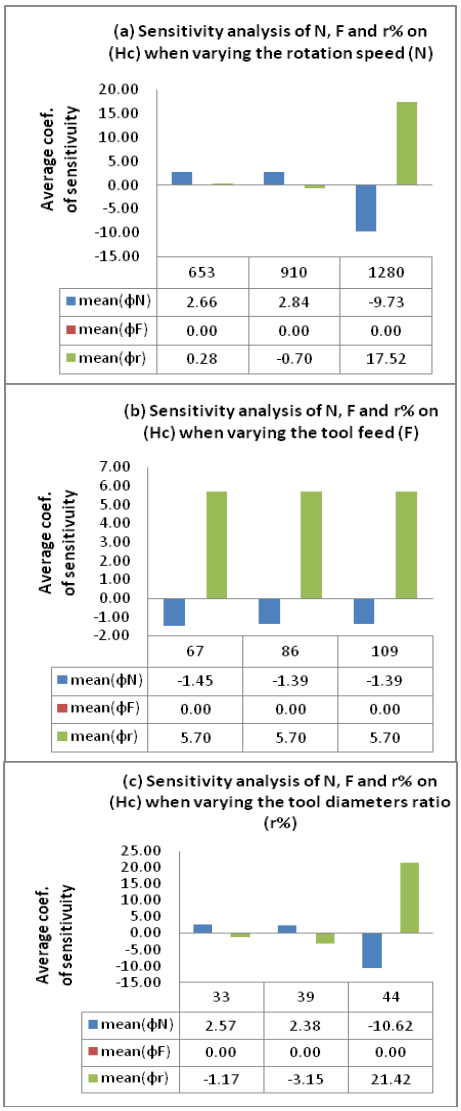

Fig. 13. Sensitivity analysis of N, F and r% on response (Hc). a) when varying the tool rotation speed (N), b) when varying the traverse rate (F), c) and, when varying the tool diameters ratio (r%)

According to the histograms showm in Fig. 13, the sensitivity analysis comes to:

- Likewise the forgoing, in average, the traverse tool rate (F) has insignificant sensitivity on the response (Hc) (ϕ_F=0.00) regardless of the setting level of the factor N, F, and/or r%.
- The histogram of Fig.13 (b) shows that the sensitivity of N and r% on (Hc), (ϕ_N=-1.39) and ($\phi_{r\%}$=5.70), respectively, are almost kept constant when varying the traverse rate (F).
- Allowing for the factors N and r%, the histograms in Fig. 13a, 13b and 13c show that in average the tool diameters ratio (r%) has the greatest sensitivity on (Hc) in spite of the setting of factors N, F and r%. The highest sensitivity of N(ϕ_N=-10.62) and r% ($\phi_{r\%}$=21.42) on (Hc) are achieved at r% high. As regards the variation effect of N, the sensitivity of N and r% on (Hc) is maximum given N high.

Published By:
Blue Eyes Intelligence Engineering
and Sciences Publication (BEIESP)

- Local maximum sensitivity coefficients for N and r% on (Hc) equal -37.58 and 64.82, respectively. And, they are met for N, F and r% being set (high, low, high), (high, middle, high) or (high, high, high), respectively (see Appendix C)

IV. RESPONSE OPTIMIZATION

In the foregoing, we emphasized the contour surface, the interaction and main effects plots pertaining to the responses (E%) and (Hc) have given rise to a dilemmatic settings when maximization. On one hand, the tensile elongation (E%) is maximum given N, F and r% being set low, high and low, respectively, on the other hand, the hardening capacity (Hc) is maximum when N and F are set low and r% middle. To alleviate such a concern, we employ the simultaneous/joint optimization procedure (desirability function) [28]. Depending on whether a process response, Y_i, is to be maximized, minimized or assigned a target value, a definite class of desirability function, $d_i(Y_i)$, is utilized. Presently, the objective is to jointly maximize (E%) and (Hc), therefore, we consider the following desirability function:

$$d_i(\hat{Y}_i)\begin{cases} 0 & if \quad \hat{Y}_i(x) < L_i \\ \left(\dfrac{\hat{Y}_i(x) - L_i}{T_i - L_i}\right)^r & if \quad L_i < \hat{Y}_i(x) < T_i \\ 1 & if \quad \hat{Y}_i(x) > T_i \end{cases}$$

Where, $L_i < T_i < U_i$ are the lower, target and upper desired values for Y_i (notice, in case of maximization, T_i is chosen large enough for Y_i). The exponent, r, measures the speed/precision to get at the vicinity of the target value.

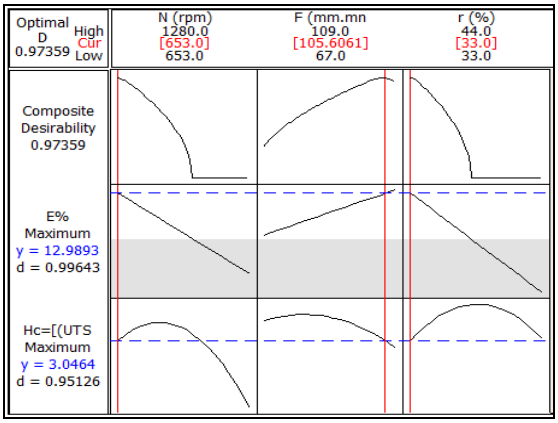

Fig. 14. Minitab® response optimizer printout

The optimal factors setting for the simultaneous maximization of (E%) and (Hc) is achieved when the composed desirability $D = \prod_{i=1}^{n} d_i^{w_i}$ comes near 1, (wi is the weight of response i).

Fig. 14. shows the Minitab® response optimizer printout. The high composed optimal desirability (D=0.97359) suggests a satisfactory solution was hit. A global optimal solution consists in setting N at 653 rpm, F at 105.606 mm.mn^{-1} and r% at 33%. The predicted process responses are then $E\%_{max}$=12.989 (desirability $d_{E\%}$=0.996) and Hc_{max}=3.046 (desirability d_{Hc}=0.951).

V. CONCLUSION AND RECOMMENDATIONS

The paper has purposed to assess the tensile elongation (E%) and the hardening capacity (Hc) in FSWed joints of the 2017 AA plates. Given the investigation space of the operating recipe (factors space), we addressed twofold goals i) search for the predictive models pertaining to the process responses (E%) and (Hc), ii) and, finding out the optimal parameters setting which would maximize (E%) and (Hc), simultaneously. Following are important study findings.

1. The Anovas and summary of fit tables (Appendices A & B) have highlighted the statistical influence of the N, r% and Fxr% terms on the tensile elongation (E%) estimate and the N, r%, Nxr% and N^2 terms on (Hc). The traverse rate (F), however, has proven irrelevant to the variation in (Hc). The maximum tensile elongation and hardening capacity which occurred in joints are about 60% and 6.8 times that found in the BM. Accordingly, both the experimental tensile elongation and hardening capacity curves of the tested coupons were very low compared with those of the BM. It turns out a fair weld ability of the 2017AA given the N, F and r% parameters spaces. Nevertheless, when increasing N, the variation in (σ_{UTS}) and (σ_{YS}) and (E%) did not disclose any softening effect.
2. In average, the sensitivity analysis of factors N, F and r% on the responses (E%) and (Hc) has emphasized the influence of the tool diameters ratio factor (r%). The sensitivity of the tool rotation speed (N) seconded r% in terms of prevalence. The FSW process sensitivity, however, was robust *vis-à-vis* the tool traverse rate factor (F).
3. The desirability study have shown that maximum elongation (E%) and hardening capacity (Hc) happened for a predicted E%=12.989 (desirability $_{dE\%}$=0.996) and Hc=3.046 (desirability $_{dHc}$=0.951). This solution holds when both N and r% are set low and F set at 105.606 mm.mn^{-1}.

Given the factors space regions, the study findings have shown that both the tool geometry (r%) and the rotation speed (N) prevail as to the variation in the (E%) and (Hc) responses, indistinctly.

VI. APPENDIX

Appendix A (E% regression model in N, F, r%)

1. *Parameter Estimate (Full Linear + Interaction Model)*				
Term	**Coef.**	**SE Coef.**	**T**	**P**
Constant	6.842	0.249	27.419	0.000
N (rpm)	-2.905	0.330	-8.812	0.000
F (mm.mn^{-1})	0.364	0.332	1.098	0.296
r (%)	-2.020	0.332	-6.090	0.000
N (rpm)xF (mm.mn-1)	0.345	0.370	0.934	0.370
N (rpm)xr (%)	-0.006	0.370	-0.017	0.987
F (mm.mn-1)x r(%)	-1.447	0.370	-3.905	0.002

2. *Summary of Fit (Full Linear + Interaction Model)*		
S = 1.050	R-Sq = 92.25%	R-Sq(adj) = 88.02%
R-Sq(pred) = 17.06%	PRESS = 129.643	Cv = 0.65

3. *ANOVA & LoF (Full Linear + Interaction Model)*						
Source	**DF**	**Seq SS**	**Adj SS**	**Adj MS**	**F**	**P**

Published By:
Blue Eyes Intelligence Engineering and Sciences Publication (BEIESP)

Regression	6	144.185	144.185	24.031	21.81	0.000
Linear	3	126.394	127.316	42.439	38.52	0.000
Interaction	3	17.791	17.791	5.930	5.38	0.016
Residual error	11	12.118	12.118	1.102	-	-
Lack-of-Fit	8	10.856	10.856	1.357	3.23	0.182
Pure Error	3	1.262	1.262	0.421	-	-
Total	17	156.303	-	-	-	-

4. *Parameter Estimate (Reduced Model)*

Term	Coef.	SE Coef.	SE Coef.	SE Coef.
Constant	6.843	0.238	28.694	0.000
N (rpm)	-2.912	0.315	-9.247	0.000
F (mm.mn-1)	0.351	0.317	1.110	0.287
r (%)	-2.019	0.317	-6.377	0.000
F (mm.mn-1)xr (%)	-1.448	0.354	-4.090	0.001

5. *Summary of Fit (Reduced Model)*

S = 1.003	R-Sq = 91.63%	R-Sq(adj) = 89.06%
R-Sq(pred) = 75.11%	PRESS = 38.904	Cv = 0.65

6. *ANOVA & LoF (Reduced Model)*

Source	DF	Seq SS	Adj SS	Adj MS	F	P
Regression	4	143.223	143.223	35.806	35.59	0.000

N(rpm)	F(mm.mn^{-1})	r %	$\hat{E}$ (%)	Coef. of Sensitivity on (E%) ϕ_N	ϕ_F	$\phi_{r\%}$	$\widehat{Hc}$	Coef. of Sensitivity on (Hc) ϕ_N	$\phi_{r\%}$
653	67	33	11.33	-0.54	0.51	-0.30	***3.44***	2.30	0.21
		39	10.92	-0.56	0.06	-0.37	2.92	2.71	0.29
		44	10.58	-0.57	-0.33	-0.43	3.03	2.61	0.31
	86	33	13.28	-0.46	0.55	-0.85	2.79	2.84	0.26
		39	11.51	-0.53	0.08	-1.16	2.92	2.71	0.29
		44	10.03	-0.61	-0.45	-1.50	3.03	2.61	0.31
	109	33	***15.65***	-0.39	0.60	-1.33	2.79	2.84	0.26
		39	12.22	-0.50	0.09	-2.01	2.92	2.71	0.29
		44	9.36	-0.65	-0.61	-2.96	3.03	2.61	0.31
910	67	33	9.01	-0.94	0.64	-0.38	2.96	2.57	-0.53
		39	8.61	-0.98	0.08	-0.47	2.68	2.84	-0.70
		44	8.26	-1.02	-0.42	-0.55	2.44	3.12	-0.87
	86	33	10.97	-0.77	0.67	-1.03	2.96	2.57	-0.53
		39	9.19	-0.92	0.10	-1.45	2.68	2.84	-0.70
		44	7.71	-1.10	-0.58	-1.95	2.44	3.12	-0.87
	109	33	13.34	-0.63	0.70	-1.56	2.96	2.57	-0.53
		39	9.91	-0.85	0.11	-2.48	2.68	2.84	-0.70
		44	7.05	-1.20	-0.81	-3.94	2.44	3.12	-0.87
1280	67	33	5.68	-2.09	1.01	-0.60	1.53	2.48	-3.21
		39	5.28	-2.25	0.13	-0.77	0.64	5.92	-9.05
		44	4.94	-2.41	-0.71	-0.93	-0.10	***-37.58***	***64.82***
	86	33	7.64	-1.56	0.96	-1.48	1.53	2.48	-3.21
		39	5.86	-2.03	0.15	-2.28	0.64	5.92	-9.05
		44	4.38	-2.71	-1.02	-3.43	-0.10	***-37.58***	***64.82***
	109	33	10.01	-1.19	0.93	-2.08	1.53	2.48	-3.21
		39	6.58	-1.81	0.17	-3.74	0.64	5.92	-9.05
		44	3.72	***-3.20***	***-1.53***	***-7.46***	-0.10	***-37.58***	***64.82***

Linear	3	126.394	127.654	42.551	42.29	0.000
Interaction	1	16.829	16.829	16.829	16.73	0.001
Residual error	13	13.080	13.080	1.006	-	-
Lack-of-Fit	10	11.818	11.818	1.182	2.81	0.214
Pure Error	3	1.262	1.262	0.421	-	-
Total	17	156.303	-	-	-	-

7. *Estimated Regression Coefficients For E% (Uncoded Data)*

Term	Coef.
Constant	-13.986
N (rpm)	-0.009
F (mm.mn^{-1})	0.499
r%	0.736

Appendix B (Hc regression model in N, F, r%)

1. *Parameter Estimate (Full Linear + Interaction Model)*

Term	Coef.	SE Coef.	T	P
Constant	3.243	0.124	26.173	0.000
N (rpm)	-0.894	0.096	-9.306	0.000
F (mm.mn^{-1})	-0.109	0.096	-1.138	0.288
r (%)	-0.361	0.096	-3.756	0.006
N^2	-0.428	0.191	-2.236	0.056
F^2	-0.162	0.186	-0.867	0.411
$r\%^2$	-0.335	0.186	-1.801	0.109
N (rpm)xF (mm.mn-1)	0.134	0.107	1.254	0.245
N (rpm)xr (%)	-0.466	0.107	-4.359	0.002
F (mm.mn-1)xr (%)	-0.114	0.107	-1.066	0.317

2. *Summary of Fit (Full Quadratic Model)*

S = 0.304	R-Sq = 95.35%	R-Sq(adj) = 90.13%
R-Sq(pred) = 61.06%	PRESS = 6.18780	Cv = 0.21

3. *ANOVA & LoF (Full Linear + Interaction Model)*

Source	DF	Seq SS	Adj SS	Adj MS	F	P
Regression	9	15.154	15.154	1.684	18.25	0.000
Linear	3	10.527	9.416	3.139	34.01	0.000
Interaction	3	2.617	2.587	0.862	9.34	0.005
Square	3	2.009	2.009	0.669	7.26	0.011
Residual error	8	0.738	0.738	0.092	-	-
Lack-of-Fit	5	0.607	0.607	0.121	2.79	0.214
Pure Error	3	0.131	0.131	0.043	-	-
Total	17	15.892	-	-	-	-

4. *Parameter Estimate (Reduced Model)*

Term	Coef.	SE Coef.	SE Coef.	SE Coef.
Constant	3.134	0.133	23.468	0.000
N (rpm)	-0.897	0.114	-7.877	0.000
r (%)	-0.348	0.114	-3.059	0.009
N^2	-0.715	0.178	-4.023	0.001
N(rpm)xr (%)	-0.467	0.127	-3.687	0.003

5. *Summary of Fit (Reduced Model)*

S = 0.360	R-Sq = 89.40%	R-Sq(adj) = 86.14%
R-Sq(pred) = 80.36%	PRESS = 3.122	Cv = 0.21

6. *ANOVA & LoF (Reduced Model)*

Source	DF	Seq SS	Adj SS	AdjMS	F	P
Regression	4	14.208	14.208	3.552	27.42	0.000
Linear	2	10.330	9.257	4.628	35.72	0.000
Square	1	2.117	2.097	2.097	16.18	0.001
Interaction	1	1.761	1.761	1.761	13.59	0.003
Residual error	13	1.684	1.684	0.130	-	-
Lack-of-Fit	4	0.545	0.545	0.136	1.08	0.423
Pure Error	9	1.139	1.139	0.127	-	-
Total	17	15.892	-	-	-	-

7. *Estimated Regression Coefficients For Hc (Uncoded Data)*

Term	Coef.
Constant	-8.548
N (rpm)	0.022
r%	0.199
N^2	-7.280E-06
N x r%	-2.710E-04

Appendix C (Normalized sensitivity Coef., $\phi_{N,F,r\%}$)

REFERENCES

[1] W. M. Thomas, E. D. Nicholas, J. C. Needham, M. G. Murch, S. P. Temple, C. J. Dawes, "Improvements relating to friction welding," G. B. Patent No. 9125978. 8, 1991.

[2] M. P. Milles, B. J. Decker, T. W. Nelson, "Formability and strength of friction-stir-welded aluminum sheets," Metallurgical And Materials Transactions, Vol. 35A, pp. 3461-3468, 2004.

[3] D. M. Rodrigues, A. Loureiro, C. Leitao, R. M. Leal, B. M. Chaparro, P. Vilaça "Influence of friction stir welding parameters on the microstructural and mechanical properties of AA6016-T4 thin welds", Materials and Design, Vol. 30, pp. 1913-1921, 2009.

[4] R. S. Mishra, Z. Y. Ma, "Friction stir welding and processing", Mater. Sci. Engr., R 50, pp. 1-78, 2005.

Published By:
Blue Eyes Intelligence Engineering
and Sciences Publication (BEIESP)

[5] R. Rai, A. De, H. K. D. H. Bhadeshia, T. DebRoy, "Review: friction stir welding tools", Science and Technology of Welding and Joining,Vol 16, pp. 325-342, 2011

[6] R. Nandan, T. DebRoy, H. K. D. H. Bhadeshia, "Recent advances in friction-stir welding–Process, weldment structure and properties," Progress in Materials Science, Vol.53,pp. 1913-1921, 2008.

[7] T. P. Chen, W.-B. Lin, "Optimal FSW process parameters for interface and welded zone toughness of dissimilar aluminum–steel joint", Science and Technology of Welding and Joining, Vol. 15, pp. 279-285, 2010.

[8] G. H. Payganeh, N. B. Mostafa Arab, Y. Dadgar Asl, F. A. Ghasemi, M. S. Boroujeni, "Effects of friction stir welding process parameters on appearance and strength of polypropylene composite welds", International Journal of the Physical Sciences, Vol. 6, pp. 4595-4601, 2011.

[9] J. Q. Li, H. J. Liu, "Effects of tool rotation speed on microstructures and mechanical properties of AA2219-T6 welded by the external non-rotational shoulder assisted friction stir welding", Materials and Design, Vol. 43, pp. 299-306, 2013.

[10] A. Razal, K. Manisekar, V. Balasubramanian, "Influences of welding speed on tensile properties of friction stir welded AZ61A magnesium alloy", Journal of Materials Engineering and Performance, Vol. 21, pp. 257-265, 2012.

[11] S. Lim, S. Kim, C. Lee, S. Kim, "Tensile behavior of friction-stir-welded Al6061-T651", Metallurgical and Materials Transactions, Vol. 35A, pp. 2829-2835, 2004.

[12] K. Elangovan, V. Balasubramanian, "Influences of pin profile and rotational speed of the tool on the formation of friction stir processing zone in AA2219 aluminum alloy, "Materials Science and Engineering A, Vol. 459, pp. 7-18, 2007.

[13] S. Rajakumar, C. Muralidharan, V. Balasubramanian, "Influence of friction stir welding process and tool parameters on strength properties of AA7075-T6 aluminum alloy joints, "Materials and Design, Vol. 32, pp. 535-549, 2011.

[14] B. Parida, M. Mohapatra, P. Biswas, N. R. Mandal, "Study of mechanical and micro-structural properties of friction stir welded Al-alloy", International Journal of Emerging Technology and Advanced Engineering, Vol. 2, pp. 307-312, 2012.

[15] C. Bitondo, U. Prisco, A. Squilace, P. Buonadonna, G. Dionoro, "Friction-stir welding of AA 2198 butt joints: mechanical characterization of the process and of the welds through DOE analysis", Int. J. Adv. Manuf. Technol., Vol. 53, pp. 505-516, 2011

[16] H. K. Mohanty, D. Venkateswarlu, M. Mahapatra, N. R. Kumar, "Modeling the effects of tool probe geometries and process parameters on friction stirred aluminium welds", Journal of Mechanical Engineering and Automation, Vol. 2, pp. 74-79, 2012.

[17] S. Rajakumar, C. Muralidharan, V. Balasubramanian, "Establishing empirical relationships to predict grain size and tensile strength of friction stir welded AA 6061-T6 aluminum alloy joints", Trans. Nonferrous Met. Soc. China, Vol.20, pp. 1863-1872, 2010.

[18] S. Rajakumar, V. Balasubramanian, "Multi-response optimization of friction-stir-welded AA1100 aluminum alloy joints", Journal of Materials Engineering and Performance, Vol. 21, pp. 809-822, 2012.

[19] R. Palanivel, P. K. Mathews, N. Murugan, "Development of mathematical model to predict the mechanical properties of friction stir welded AA6351 aluminum alloy", Journal of Engineering Science and Technology Review, Vol. 4, pp. 25-31, 2011.

[20] A. K. Lakshminarayanan, V. Balasubranian, "Process parameters optimization for friction stir welding of RDE-40 aluminum alloy using Taguchi technique", Transaction of non-ferrous alloys of china, Vol. 18, pp. 548-554, 2008.

[21] A. S. Vagh, S. N. Pandya, " Influence of process parameters on the mechanical properties of friction stir welded AA2014-T6 Alloy using Taguchi orthogonal array", International Journal of Engineering Sciences & Emerging Technologies, Vol. 2, pp. 51-58, 2012.

[22] K. Brahma Raju, N. Harsha, V. K. Viswanadha Raju, "Prediction of tensile strength of friction steer welded joints using artificial neural networks", International Journal of Engineering Research & Technology, Vol. 1 pp. 1-5, 2012.

[23] I. N. Tansel, M. Demetgul, H. Okuyucu, A. Yapici, "Optimizations of friction stir welding of aluminum alloy by using genetically optimized neural network", Int. J. Adv. Manuf. Technol., Vol. 48, pp. 95-101, 2010.

[24] H. J. Liu, H. Fujii, M. Maedaa, K. Nogi, "Tensile properties and fracture locations of friction-stir-welded joints of 2017-T351 aluminum alloy", Journal of Materials Processing Technology, Vol. 142, pp. 692-6996, 2003.

[25] A. Mirjalil, H. J. Aval, S. Serajzadeh, A.H. Kokabi, "Microstructural evolution and mechanical properties of FSWed 2017 AA with different initial microstructures", Proceedings of Institution of Mechanical Engineers, Part L: Journal of Material Design and Applications, February 2013.

[26] M. Rezgui, A. Trabelsi, M. Ayadi, and H. Bouzaiene, "RSM Modeling for Predicting Ultimate Tensile Stress and Yield Stress in Friction Steer Welded Aluminum 2017 A", submitted to Trans. Nonferrous Mat. Soc. China, 2013.

[27] C. Douglas, C. Montgomery, "Design and Analysis of Experiments", Sixth Edition, John Wiley and Sons, Inc. 2005.

[28] G. Derringer, R. Suich, "Simultaneous optimization of several response variables", J. of Quality Technology, Vol. 5, pp. 469-479, 1980.

Dr. Ali TRABELSI gained a PhD (1995) in Manufacturing Systems from the “Ecole Centrale de Paris” in association with the University of Dundee. His research interests are tolerancing for non conventional machining and forming processes.

Dr. Mohamed-Ali REZGUI gained a PhD in Mechanical Engineering from the “Ecole Centrale de Lyon”, France. His research activities are thermo-forming and simulation/modeling of material behavior (aluminum, polymers).

Dr. Smain BEZZINA obtained in 1996 a PhD in Mechanical Engineering from the Compiegne University of Technology, France., His research fields are numerical modeling of damage mechanics and FEA techniques applied in forming processes.

Published By:
Blue Eyes Intelligence Engineering and Sciences Publication (BEIESP)